Journal of Power Sources 220 (2012) 122–129

Contents lists available at SciVerse ScienceDirect

Journal of Power Sources

journal homepage: www.elsevier.com/locate/jpowsour

Sol–gel synthesis of Li_2CoPO_4F/C nanocomposite as a high power cathode material for lithium ion batteries

Xiaobiao Wu [a], Zhengliang Gong [b], Shi Tan [a], Yong Yang [a,b,*]

[a] State Key Laboratory for Physical Chemistry of Solid Surfaces, and Department of Chemistry, College of Chemistry and Chemical Engineering, Xiamen University, Xiamen 361005, China
[b] School of Energy Research, Xiamen University, Xiamen 361005, China

HIGHLIGHTS

- Li_2CoPO_4F/C nanocomposite was successfully synthesized by sol–gel method.
- The uniformly carbon coated Li_2CoPO_4F particles are only tens of nanometers.
- Li_2CoPO_4F/C cathode material delivers 138 mAh g^{-1} at 1 C and 119 mAh g^{-1} at 20 C.
- $Li_2CoPO_4F/Li_4Ti_5O_{12}$ full cells show impressive electrochemical performance.

ARTICLE INFO

Article history:
Received 21 January 2012
Received in revised form
9 June 2012
Accepted 31 July 2012
Available online 8 August 2012

Keywords:
Lithium cobalt fluorophosphate
Lithium ion batteries
Sol–gel method
High power density

ABSTRACT

Li_2CoPO_4F cathode materials are successfully synthesized by solid state (SS) and sol–gel (SG) methods. The XRD results show that Li_2CoPO_4F samples prepared by two methods are both indexed as orthorhombic structure with space group P*nma*. The particles of Li_2CoPO_4F (SS) are micron grade. However, the particle of Li_2CoPO_4F (SG) is only tens of nanometers with an amorphous carbon uniformly coated. A high reversible capacity of 138 mAh g^{-1} is achieved for Li_2CoPO_4F/C (SG) at 1 C, which is much higher than that of 106 mAh g^{-1} prepared by solid state method. Also, Li_2CoPO_4F/C (SG) shows excellent rate performance, a capacity of 119 mAh g^{-1}, 86% retention of that at 1 C, is achieved at 20 C. The excellent rate capacity of the material is attributed to nanosized particles and uniform carbon coating that reduce ion diffusion length and enhance electronic conductivity. Furthermore, the preliminary performance characteristics of $Li_2CoPO_4F/Li_4Ti_5O_{12}$ full cells are presented. The cell shows a high voltage plateau around 3.4 V with excellent rate capacity. The impressive electrochemical properties indicate that Li_2CoPO_4F can be a promising high power cathode material for lithium ion batteries. The capacity fading mechanism of Li_2CoPO_4F is also briefly investigated.

1. Introduction

Lithium ion batteries have been successfully applied to portable equipments since the first commercialization of them in 1990s. Extensive studies have been devoted to exploring and developing new materials to meet the ever-increasing requirements on high energy & power density batteries, especially for hybrid electric vehicle (HEV) and electric vehicle (EV) applications [1]. $LiFePO_4$ is considered to be one of the promising candidate cathode materials for large-scale lithium ion batteries due to its good thermal and structural stability [2]. Normally, carbon-based anode materials are not suitable for high rate lithium intercalation process due to safety problem originated from Li dendrite deposition. Some recently developed anode materials with relatively higher voltage plateau, for example $Li_4Ti_5O_{12}$ and TiO_2 [3,4], can be good replacements for carbon to further improve the safety of large-scale lithium ion batteries. For example, $LiFePO_4/Li_4Ti_5O_{12}$ full cell demonstrated impressive rate capacity and safety [5]. However, its operation voltage is only around 1.9 V, which seriously decreases the energy density of Li-ion batteries. In order to improve the energy density and the safety of lithium ion batteries, the development of high voltage cathode materials (5 V or higher) and the combination with Ti-based anode materials can be a good choice. Recently, fluorophosphates A_2MPO_4F (A = Li, Na; M = Mn, Fe, Co) have been proposed as promising high voltage cathode materials not only because of the inducing effect of PO_4^{3-} group but also the high

* Corresponding author. State Key Laboratory for Physical Chemistry of Solid Surfaces, and Department of Chemistry, College of Chemistry and Chemical Engineering, Xiamen University, Room 408, Chemistry Building, Xiamen 361005, China. Tel./fax: +86 592 2185753.
E-mail address: yyang@xmu.edu.cn (Y. Yang).

0378-7753/$ – see front matter © 2012 Elsevier B.V. All rights reserved.
http://dx.doi.org/10.1016/j.jpowsour.2012.07.099

electronegativity of F^- anion [6–11]. High capacity may also be achieved in A_2MPO_4F with the extraction/insertion of more than one lithium ion *via* $M^{2+}/M^{3+}/M^{4+}$ redox couples, which has been demonstrated recently in $Na_2Fe_{1-x}Mn_xPO_4F$ serial materials [12]. Among them, Li_2CoPO_4F was found to show a redox potential of ~5 V vs. Li/Li^+, which is one of the highest among currently available cathodes. Also, Li_2CoPO_4F was found to possess good chemical stability, thermal stability and structural stability [10,13]. The high operating voltage, high theoretical capacity combined with good stability make it an interesting candidate cathode material for high energy density Li-ion batteries. Also, when combined with $Li_4Ti_5O_{12}$ anode, Li_2CoPO_4F will significantly improve the operation voltage of the result cells.

Several works have already been devoted to the synthesis and structure analysis of Li_2CoPO_4F [10,13–16]. However, there are only few articles about the electrochemical performances of Li_2CoPO_4F so far [14,17]. Sub-micron Li_2CoPO_4F prepared by Wang et al. using a solid state method delivers a discharge capacity of 109 mAh g^{-1} at a current density of 5 mA g^{-1} over the voltage rang of 2–5.5 V [14]. Meanwhile, Dumont-Botto et al. [17] prepared a sub-micron Li_2CoPO_4F using a Spark Plasma Sintering technique, which exhibited a capacity of around 110 mAh g^{-1} at C/10 over the voltage rang of 2–5.5 V. However, these works only reported the electrochemical performance at low current density without giving the rate capability, which may be due to the low electronic conductivity of polyanionic compounds [2,9,18]. *In situ* carbon coating is an effective technique to improve the electronic conductivity and obtain small particles *via* inhibiting the particles growth and aggregation, which has been successfully demonstrated on many low conductive electrode materials [19]. However, for cobalt-based materials, *in situ* carbon coating may be unachievable due to the reduction of Co^{2+} to Co metal when pyrolyzing the carbon precursors, thus should be treated very carefully [20]. Therefore, it is worthy to investigate that whether carbon can be successfully coated on particle surface of Li_2CoPO_4F to enhance electrochemical performances.

In this study, we present a sol–gel approach to synthesize Li_2CoPO_4F/C nanocomposite cathode material for the first time. *In situ* carbon coating is successfully achieved on Li_2CoPO_4F *via* optimizing the synthesis conditions. Nano-Li_2CoPO_4F with uniform carbon coating layer is obtained. Its electrochemical performances are compared with Li_2CoPO_4F prepared by solid state method. In the meantime, the electrochemical performances of $Li_2CoPO_4F/Li_4Ti_5O_{12}$ full cells are investigated. The capacity fading mechanism of Li_2CoPO_4F upon cycling is also briefly studied and discussed.

2. Experimental

The Li_2CoPO_4F/C nanocomposite was synthesized by sol–gel (SG) method. In brief, 0.01 mol $Co(NO_3)_2{\cdot}6H_2O$, 0.01 mol H_3PO_4 (85 wt% solution), 0.02 mol LiF, and 0.02 mol citric acid were dissolved in 50 ml deionized water, and the mixture was stirred at 80 °C for 24 h. Then 1.8 ml ethylene glycol was added into the solution and kept at 120 °C for another 2 h. The solution was transported to a culture dish and dried at 100 °C overnight to get the precursor. The precursor was ground and pressed into pellets, then sintered at 600 °C for 6 h in an argon atmosphere. The carbon content of the Li_2CoPO_4F/C (SG) nanocomposite was determined to be 12.2 wt% by Vario EL III elemental analyzer (Elementar Analysen System GmbH, Germany).

For comparison, Li_2CoPO_4F was also synthesized by solid state (SS) method. It was similar to the method that had been reported by Wang et al. [14]. A mixture of 0.01 mol $CoAc_2{\cdot}4H_2O$, 0.01 mol $NH_4H_2PO_4$ and 0.02 mol LiF was ball milled at a speed of 500 rpm for 10 h using acetone as a dispersant. After evaporated the solvent, the mixture was pressed into pellets, then heat treated at 650 °C for 6 h in an argon atmosphere.

The crystalline phase of the samples was collected by Panalytical X-pert diffractometer (PANalytical, Netherlands) equipped with Cu Kα radiation operated at 40 kV and 30 mA. Scanning electron microscopy (SEM) was studied by S-4800 (HITACHI, Japan), with energy-dispersive spectroscopy (EDS). The transmission electron microscopy (TEM) and high resolution transmission electron microscopy (HRTEM) were studied by JEM-2100 (JEOL Ltd., Japan) at 200 kV.

Electrochemical performance of the cathode materials was examined using CR2025 coin-type cells. The cathode electrodes were fabricated with 70 wt% active material, 20 wt% acetylene black and 10 wt% poly(vinylidene fluoride) (PVDF) using N-methyl-2-pyrrolidone (NMP) as the solvent. The electrodes were prepared by coating the slurry on the aluminum current collector with a diameter of 1.6 cm, and dried at 120 °C for 1 h. The electrode contained 2–3 mg of active cathode material. The as prepared electrode, lithium metal, 1 M $LiPF_6$ in EC/DMC (1:1, v/v) or 1 M $LiPF_6$ in dimethyl sulfone (DMS) and ethyl methyl sulfone (EMS) (15:85, w/w) [14], and Celgard 2300 were used as cathode, anode, electrolyte and separator respectively to assemble cells in an argon-filled glove box. The DMS (98%, Aldirch) and EMS (98%, TCI) were firstly mixed together, and then treated with molecular sieve (4A) to eliminate water residue in the solvents before further preparing the sulfone-based electrolyte solution. For $Li_2CoPO_4F/Li_4Ti_5O_{12}$ full cells, $Li_4Ti_5O_{12}$ replaces lithium metal as anode. The $Li_4Ti_5O_{12}$ anode electrode was prepared in the same way as the cathode electrode except mixing the active material, acetylene black and PVDF in a weight ratio of 80:10:10. The full cells were designed to be cathode limited, and the amount of anode material was in excess to cathode material (the mass ratio of Li_2CoPO_4F and $Li_4Ti_5O_{12}$ in the full cell was controlled between 1:1.6 ~ 1.8, in another word, the capacity of $Li_4Ti_5O_{12}$ anode was around twice that of Li_2CoPO_4F cathode (calculated based on the theoretical capacity of Li_2CoPO_4F cathode and $Li_4Ti_5O_{12}$ anode)). Charge/discharge performance of the materials was investigated galvanostatically between 2 and 5.4 V for Li_2CoPO_4F/Li half cells and 0.5–3.9 V for $Li_2CoPO_4F/Li_4Ti_5O_{12}$ full cells at *n C* current rate ($1C = 143$ mA g^{-1}, $n = 1, 2, 5, 10, 20$) at 30 °C (Land CT2001A). The charge/discharge capacity was calculated based on the mass of Li_2CoPO_4F.

Ex situ XRD was carried out to determine the structure changes after different charge/discharge cycles. After different charge/discharge cycles, the cells were disassembled and washed by DMC in the argon-filled glove box. Electrochemical impedance spectroscopy (EIS) of the cell was measured at the charged state of 4.9 V after different cycles over frequency range from 100 kHz to 10 mHz with a perturbation amplitude of ±5 mV using Autolab workstation (Eco Chemime, Netherlands).

3. Results and discussion

Fig. 1 shows the XRD patterns of Li_2CoPO_4F (SG) sintered at different temperatures for 6 h. The diffraction peaks of the sample sintered at 550 °C are mostly indexed to $LiCoPO_4$ and LiF, and a small amount of Li_2CoPO_4F is also present. When the sintering temperature is increased to 600 °C, the predominant phase becomes Li_2CoPO_4F with trace of $LiCoPO_4$ as impurity. $LiCoPO_4$ as an impurity disappears when increasing the sintering temperature to 650 °C. However, a new small diffraction peak appears at 44.2° corresponding to the diffraction peak of cobalt due to the reduction of Co^{2+} to metallic cobalt by carbon. When the sintering temperature reaches 700 °C, diffraction peaks of cobalt become more obvious, indicating that the reduction of Co^{2+} becomes severer at 700 °C. At the same time, $LiCoPO_4$ impurity appears once again,

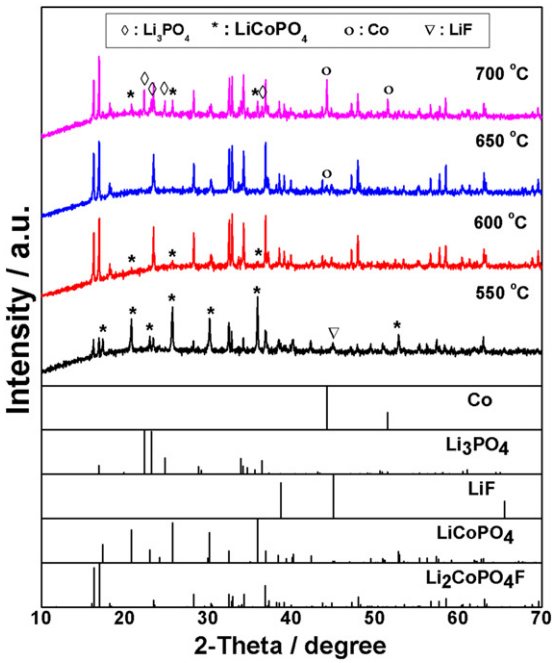

Fig. 1. XRD patterns of Li_2CoPO_4F prepared by sol–gel method sintered at 550 °C, 600 °C, 650 °C and 700 °C. The JCPDS numbers of Co, Li_3PO_4, LiF, $LiCoPO_4$ are 00-015-0806, 01-087-0039, 01-078-1217, 01-089-6192, respectively. Reference diffraction pattern of Li_2CoPO_4F is obtained from simulation based on CIF document reported by Hadermann et al. [15] using diamond 3.1 software.

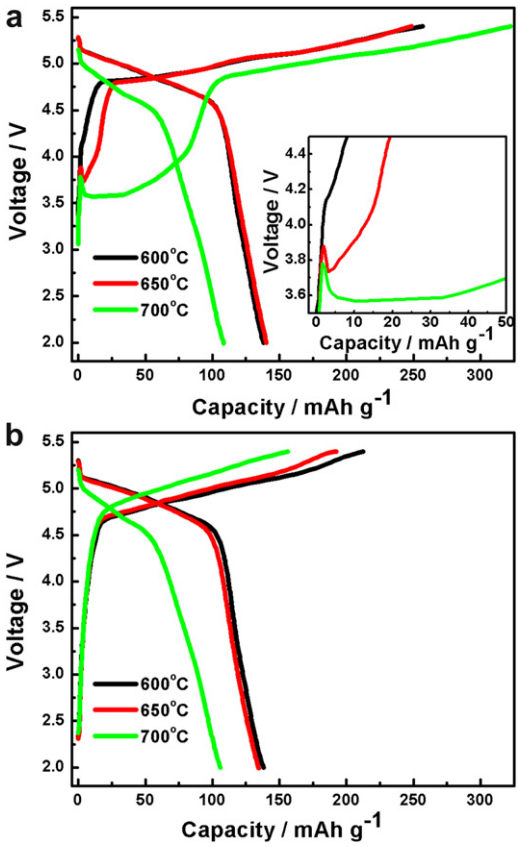

Fig. 2. The first (a) and second (b) charge/discharge profiles for half cells in $LiPF_6$/EC + DMC electrolyte of Li_2CoPO_4F prepared by sol–gel method sintered at 600 °C, 650 °C and 700 °C at 1 C current rate.

which agrees with Khasanova's results that Li_2CoPO_4F is metastable and may decompose to $LiCoPO_4$ and Li_3PO_4 at high temperature [13]. So pure phase of Li_2CoPO_4F can only exist at a narrow temperature range [16].

Fig. 2 shows the first and second charge/discharge profiles for half cells in $LiPF_6$/EC+DMC electrolyte of Li_2CoPO_4F (SG) sintered at different temperatures at 1 C current rate. A charging voltage plateau is shown at around 3.8 V in the first cycle for the sample sintered at 650 °C, and it becomes more obvious when the sintering temperature reaches 700 °C. Based on our analysis on this electrochemical system, this part of charge capacity can be ascribed to the electrochemical oxidation of metallic cobalt in the charge process. Plateaus corresponding to oxidation of metallic cobalt disappear in the second cycle. In the following cycles, no 3.8 V plateau is shown which means no oxidation reaction of cobalt happens again. Meanwhile, no 3.8 V plateau appears for the sample sintered at 600 °C, which is in accordance with XRD result that reduction of Co^{2+} to cobalt metal does not happen at 600 °C. There are no significant differences in charge/discharge profiles between the samples sintered at 600 °C and 650 °C except for the small plateau at around 3.8 V, and the electrochemical performance of the material is not seriously affected by the impurity of $LiCoPO_4$. Therefore, the sintering temperature for sol–gel method is optimized to be 600 °C.

For comparison, Li_2CoPO_4F was also prepared by a conventional solid state method. As discussed above, Li_2CoPO_4F (SG) sample sintered at 600 °C has some $LiCoPO_4$ impurity, so sintering temperature of 650 °C was chosen to synthesize Li_2CoPO_4F for solid state method. Fig. 3 shows XRD patterns of Li_2CoPO_4F prepared by solid state and sol–gel methods. No distinct impurity is detected for the sample prepared by solid state method, indicating that increasing sintering temperature contributes to the synthesis of pure phase of Li_2CoPO_4F. Except for the peaks of impurity, all peaks of Li_2CoPO_4F samples prepared by both solid state and sol–gel methods can be indexed as an orthorhombic structure with space group P*nma*. The lattice parameters of Li_2CoPO_4F prepared by solid state method calculated by Jade.5 are $a = 10.452$ Å, $b = 6.386$ Å, $c = 10.889$ Å and $V = 726.83$ Å^3. For Li_2CoPO_4F prepared by sol–gel method, the lattice parameters are $a = 10.458$ Å, $b = 6.377$ Å, $c = 10.880$ Å, $V = 725.70$ Å^3. The results we obtained above are in good agreement with the reported data [10].

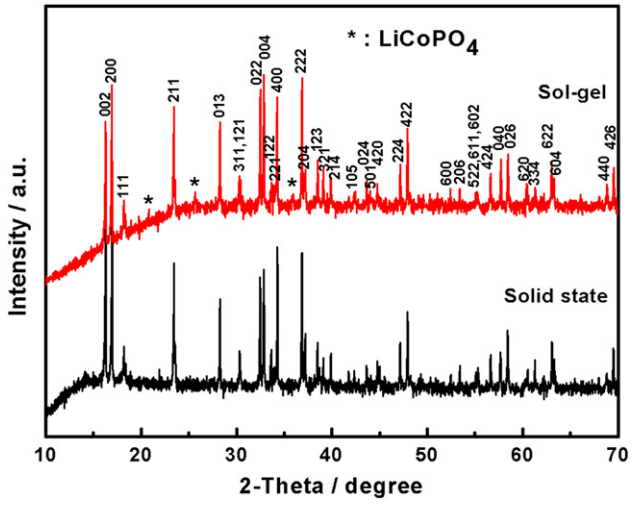

Fig. 3. XRD patterns of Li_2CoPO_4F prepared by solid state and sol–gel methods.

Fig. 4 shows SEM images of Li_2CoPO_4F prepared by solid state and sol–gel methods. It can be seen that particles of Li_2CoPO_4F prepared by solid state method are several micrometers and not uniformly distributed. Whereas Li_2CoPO_4F/C prepared by sol–gel method does show primary nanocrystallite aggregate structure. The secondary particles of Li_2CoPO_4F/C prepared by sol–gel method are a few micrometers. Under high magnification, this sample exhibits a much narrower particle size distribution with nanosized primary particles. TEM image (Fig. 5a) also indicates that the primary particle size of Li_2CoPO_4F (SG) is only tens of nanometers in accordance with the SEM results. An amorphous carbon layer coating on the surface of the particles can be observed from HRTEM image (Fig. 5b). It can be seen that carbon is uniformly distributed on the particle surface from EDS maps (Fig. 6), which agrees with the result of HRTEM. The nanocrystallite and uniform conductive carbon matrix reduce the diffusion path length of lithium ion and improve the electronic conductivity of the composite material. These would significantly enhance the electrochemical performance of Li_2CoPO_4F.

Fig. 7 shows the first charge/discharge profiles for half cells in $LiPF_6$/EC+DMC electrolyte of Li_2CoPO_4F prepared by solid state and sol–gel methods at various rates. Li_2CoPO_4F (SS) cathode material exhibits a discharge capacity of 106 mAh g^{-1} at 1 C current rate, which is similar to the results reported in literature [14,17]. Furthermore, the capacity decreases, accompanying with an increase in polarization when increasing the current rate. When current rate is increased to 20 C, the discharge capacity dramatically decreases to 29 mAh g^{-1} and severe polarization is also observed, which can be ascribed to the low intrinsic conductivity of polyanionic cathode materials. Li_2CoPO_4F (SG) shows a high discharge capacity of 138 mAh g^{-1} at 1 C current rate, which is very close to the theoretical capacity (143 mAh g^{-1}) calculated based on one electron exchange per formula unit. Compared with Li_2CoPO_4F (SS) sample, the most outstanding feature of Li_2CoPO_4F (SG) sample lies in its superior rate capability. When current rate reaches to 2 C and 5 C, the initial discharge capacities just slightly decrease to 135 mAh g^{-1} and 133 mAh g^{-1}, respectively, without obvious drop in discharge plateau. Even when current rate is increased to 10 C and 20 C, the discharge capacities can still reach 127 mAh g^{-1} and 119 mAh g^{-1}, corresponding to 92% and 86% of its capacity at 1 C, respectively, which are still much better than that prepared by solid state method cycled at low current density. The outstanding electrochemical performances of the composites can be attributed to the nanosized particles and uniform carbon distribution benefitting from our novel sol–gel technique. In addition, Li_2CoPO_4F/C nanocomposite exhibits high voltage plateau (~5.0 V) and excellent rate performance, thus Li_2CoPO_4F can be regarded as a promising high power cathode material for lithium ion batteries. It is worthy to mention that coulomb efficiencies of Li_2CoPO_4F samples prepared by solid state and sol–gel methods are both found to be low. Li_2CoPO_4F material must be charged to high voltage (5.4 V) to obtain high capacity due to its high redox potential, which results in some serious side decomposition reactions of electrolyte [21]. Meanwhile, the catalytic effects of cobalt ion on the decomposition of electrolyte may also contribute to its high irreversible capacity loss [22].

In order to decrease the initial irreversible capacity loss, sulfone-based electrolyte with high voltage stability window is used to investigate the electrochemical performances of Li_2CoPO_4F cathode material. Fig. 8 shows the first charge/discharge profiles of Li_2CoPO_4F (SG)/Li half cells in $LiPF_6$/DMS + EMS electrolyte at various rates. Li_2CoPO_4F cathode material exhibits a reversible discharge capacity of 132 mAh g^{-1} at 1 C in $LiPF_6$/DMS + EMS electrolyte, which is slightly lower than that in $LiPF_6$/EC + DMC electrolyte. Higher initial coulombic efficiency (67.2%) can be achieved in $LiPF_6$/DMS + EMS electrolyte in comparison with 53.8% in $LiPF_6$/EC + DMC electrolyte, which is attributed to the higher stability of $LiPF_6$/DMS + EMS electrolyte. However, when the current density is

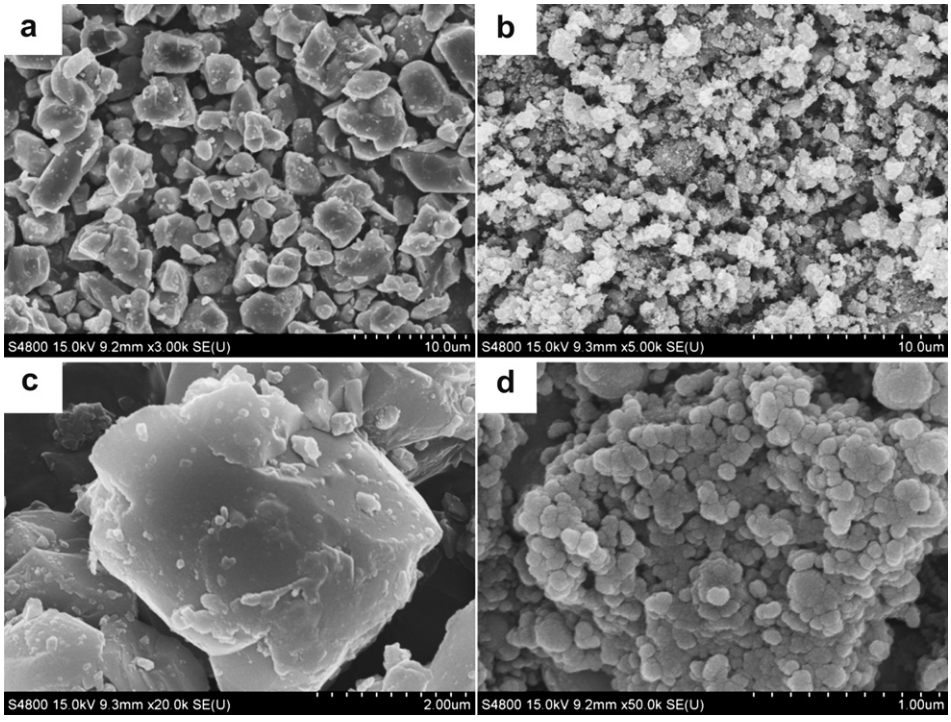

Fig. 4. SEM images of Li_2CoPO_4F prepared by solid state (a, c) and sol–gel (b, d) methods.

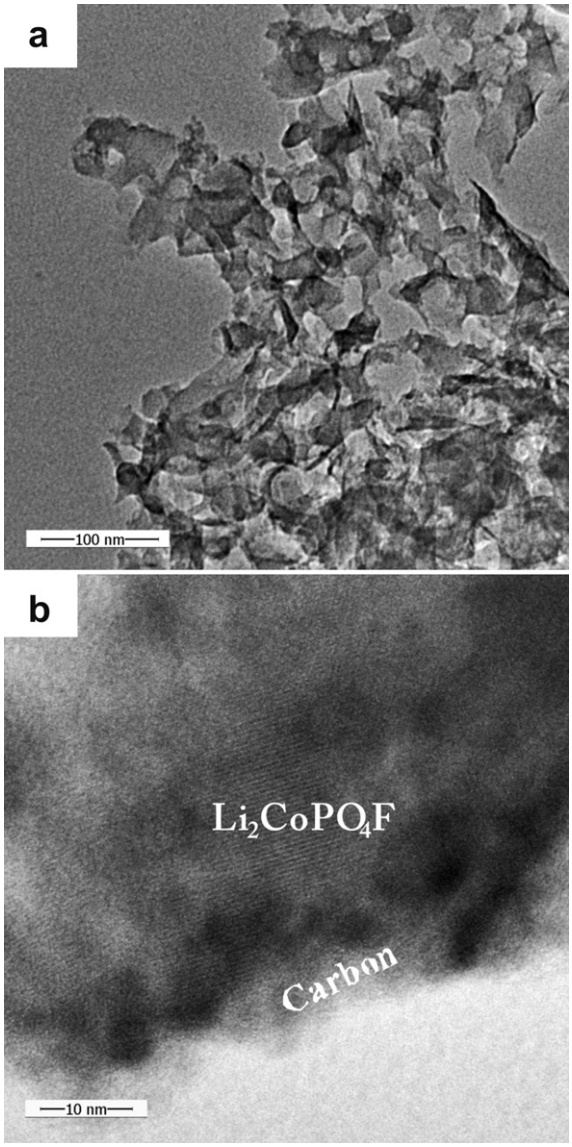

Fig. 5. TEM (a) and HRTEM (b) images of Li_2CoPO_4F prepared by sol–gel method.

increased, accompanying with an obvious decline of the discharge plateau, the first discharge capacity of the electrode material decreases sharply to only 83 mAh g^{-1} at 20 C (only 62.9% of that at 1 C) compared to 119 mAh g^{-1} in $LiPF_6$/EC + DMC electrolyte. It is speculated that $LiPF_6$/DMS + EMS electrolyte suffers from low ionic conductivity [23], which results in high electrolyte resistance and serious concentration polarization of electrolyte. Therefore, the development of high voltage electrolytes combined with high ionic conductivity, low viscosity and good wettability is critical for the practical application of these high voltage cathode materials. In the following experiments, we used $LiPF_6$/EC + DMC as electrolyte to give full play to the electrochemical performance of Li_2CoPO_4F cathode material.

Now, the commercial carbon-based anode materials suffer from safety problem when lithium ion intercalates at high current density. $Li_4Ti_5O_{12}$ anode material has excellent rate and cycling performances, whereas its charge/discharge plateau is relatively high located at 1.5 V. When $Li_4Ti_5O_{12}$ is combined with currently commercialized cathode materials, it will significantly decrease the operating voltage of the result cells. For example, $LiFePO_4$/$Li_4Ti_5O_{12}$ full cell exhibits a voltage plateau at 1.9 V, which would significantly decrease the energy density of lithium ion batteries. If a suitable high voltage electrolyte can be developed, Li_2CoPO_4F/$Li_4Ti_5O_{12}$ full cells should show superior energy density and power density. The electrochemical properties of Li_2CoPO_4F/$Li_4Ti_5O_{12}$ full cells are preliminary investigated. Fig. 9 shows the first charge/discharge profiles of Li_2CoPO_4F/$Li_4Ti_5O_{12}$ full cells in $LiPF_6$/EC + DMC electrolyte at various rates. Li_2CoPO_4F/$Li_4Ti_5O_{12}$ full cells have similar discharge capacity to Li_2CoPO_4F/Li half cells, indicating that Li_2CoPO_4F cathode material and $Li_4Ti_5O_{12}$ anode material have a good electrochemical compatibility. Li_2CoPO_4F/$Li_4Ti_5O_{12}$ full cell exhibits a voltage plateau at about 3.4 V, which leads to 78% improvement in voltage plateau compared with $LiFePO_4$/$Li_4Ti_5O_{12}$ full cell. Although the capacity of Li_2CoPO_4F/$Li_4Ti_5O_{12}$ full cell is slightly lower than that of $LiFePO_4$/$Li_4Ti_5O_{12}$ full cell, its energy density is still remarkably higher (~50%) than $LiFePO_4$/$Li_4Ti_5O_{12}$ full cell due to its high operation voltage. The high working voltage and excellent rate capability of Li_2CoPO_4F/$Li_4Ti_5O_{12}$ full cell make it a promising high power lithium ion battery which prevents the safety issues caused by the highly reactive lithiated graphite.

Fig. 10 shows the cycling performance of Li_2CoPO_4F (SG)/Li half cells in $LiPF_6$/EC + DMC electrolyte at various rates. Li_2CoPO_4F/Li half cells exhibit poor cycling performance at various rates and the capacity retention is only 36% after 50 cycles at 1 C rate. The severe capacity fading may be ascribed to the structure changes during cycling or the decomposition of electrolyte when charged to high voltage (5.4 V). In order to investigate the capacity fading mechanism, *ex situ* XRD and EIS techniques were carried out. Fig. 11 shows *ex situ* XRD patterns of Li_2CoPO_4F (SG) after different cycles. No obvious structural degradation is observed for Li_2CoPO_4F sample after 50 cycles. This indicates that Li_2CoPO_4F possesses high structural stability during charge/discharge processes. The most obvious differences in patterns between pristine Li_2CoPO_4F and Li_2CoPO_4F samples after charge/discharge cycling lie in the relative intensity change of diffraction peaks located at 16.3° and 17.0°. This phenomenon was also observed by Wang et al., which may arise from the structural relaxation when Li_2CoPO_4F is charged to a voltage above 5 V [14]. For Li_2CoPO_4F samples after different cycles (1, 10, 20, 30 40 and 50 cycles), no obvious changes are observed on their diffraction patterns. This indicates the structural relaxation is almost complete on the first charge/discharge cycle, and the structure of Li_2CoPO_4F keeps stable on the subsequent cycles. Electrochemical impedance spectroscopy (EIS) has been performed to study the interface properties during cycling. Fig. 12 shows the nyquist plots of Li_2CoPO_4F (SG)/Li half cell in $LiPF_6$/EC + DMC electrolyte at different cycles. All nyquist plots consist of three parts, the high frequency semicircle relates to solid electrolyte interface (SEI) resistance (R_{SEI}), the medium frequency semicircle relates to the charge-transfer resistance (R_{ct}) and the low frequency straight line represents the Warburg impedance (Z_w). It can be clearly seen that the charge-transfer resistance sharply increases during cycling process, while R_{SEI} is relatively stable. The fast capacity fading cannot be mainly attributed to the growth of solid electrolyte interface resistance. It is speculated that F^- anion in $LiPF_6$ contained electrolyte attacks the surface of Li_2CoPO_4F, with the result that a layer of decomposition products with poor electronic conductivity cover on the surface of Li_2CoPO_4F electrode [24]. In the meantime, the catalytic effect of cobalt ions aggravates the reaction when the electrode was charged to high voltage. Progressive damaging of the surface of Li_2CoPO_4F electrode also destroys the close contract between the surface of electrode and conductive carbon layer. These factors may result in poor charge-transfer dynamics and the fast

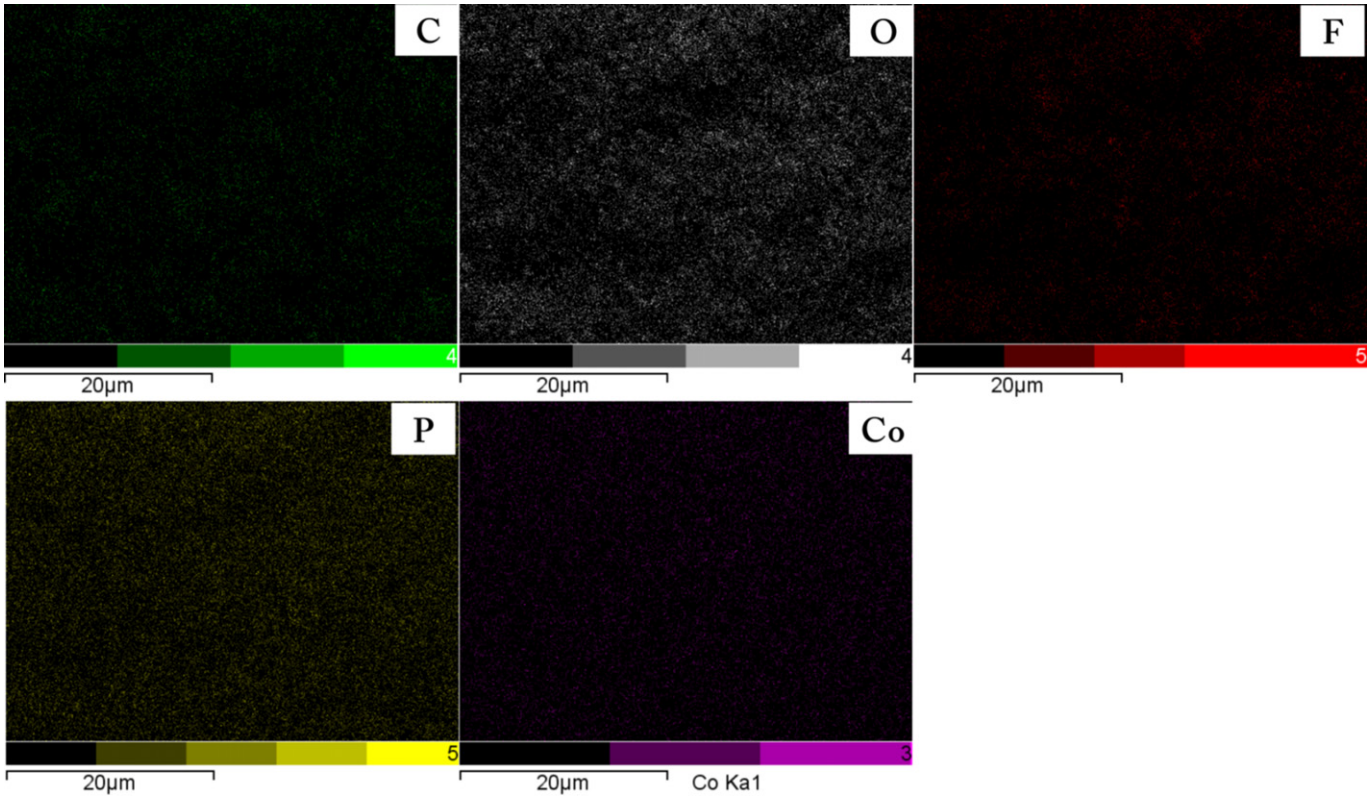

Fig. 6. EDS mapping of Li_2CoPO_4F prepared by sol–gel method.

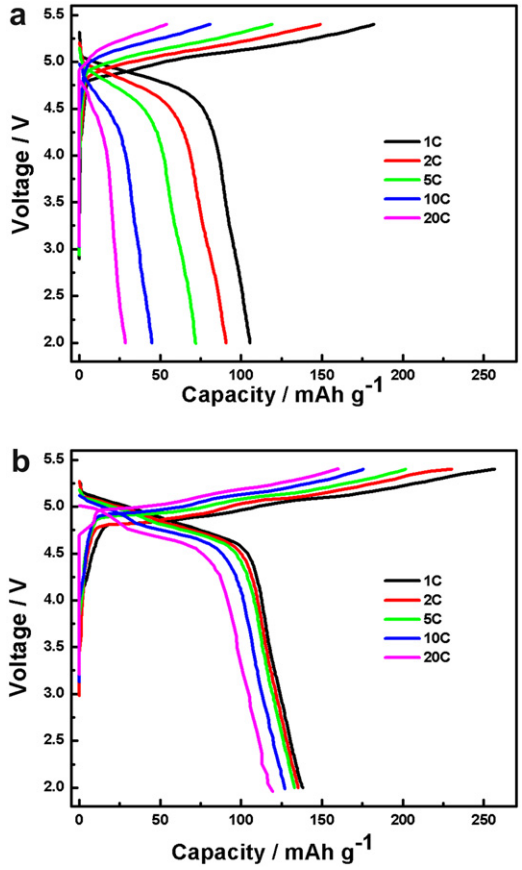

Fig. 7. The first charge/discharge profiles for half cells in $LiPF_6$/EC + DMC electrolyte of Li_2CoPO_4F prepared by solid state (a) and sol–gel (b) methods at various rates.

increase in charge-transfer resistance during charge/discharge cycling, and then decrease the discharge capacity. According to *ex situ* XRD and EIS analyses, we may conclude that the fast capacity fading is mainly ascribed to the instability of electrode/electrolyte interface during cycling at high voltage rather than structural degradation.

Fig. 13 shows the cycling performance and coulombic efficiency plots of Li_2CoPO_4F (SG)/$Li_4Ti_5O_{12}$ full cells in $LiPF_6$/EC + DMC electrolyte at various rates. It shows that the cycling performance of Li_2CoPO_4F (SG)/$Li_4Ti_5O_{12}$ full cells is similar to

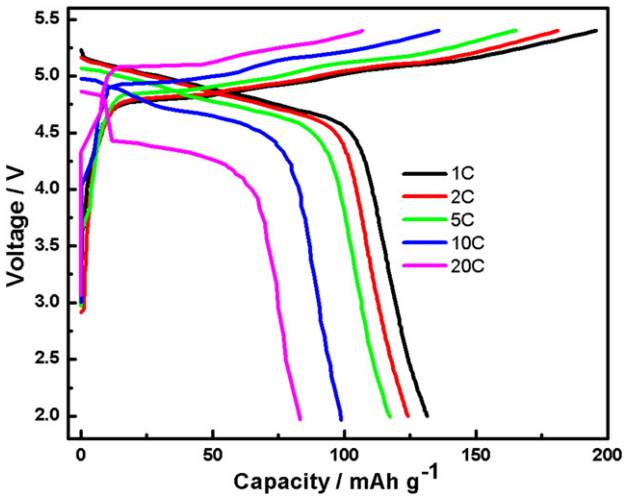

Fig. 8. The first charge/discharge profiles of Li_2CoPO_4F (SG)/Li half cells in $LiPF_6$/DMS + EMS electrolyte at various rates.

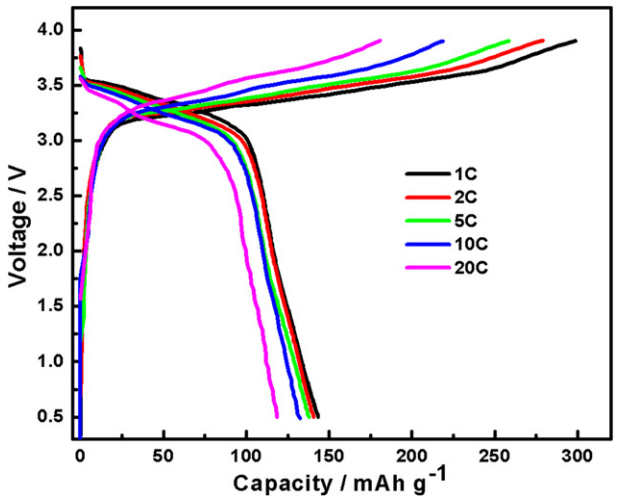

Fig. 9. The first charge/discharge profiles of Li_2CoPO_4F (SG)/$Li_4Ti_5O_{12}$ full cells in $LiPF_6$/EC + DMC electrolyte at various rates.

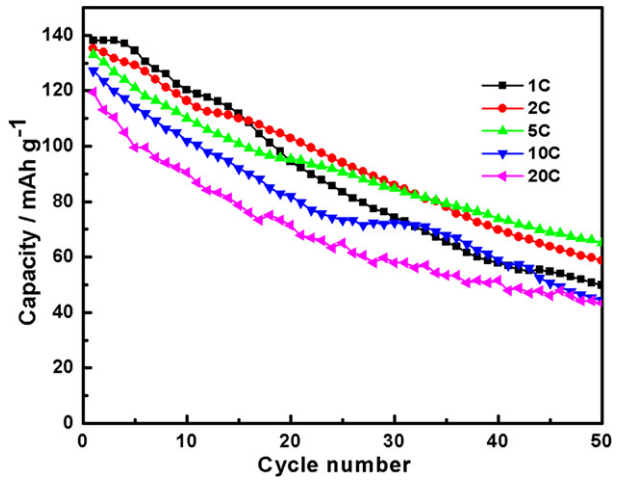

Fig. 10. Cycling performance of Li_2CoPO_4F (SG)/Li half cells in $LiPF_6$/EC + DMC electrolyte at various rates.

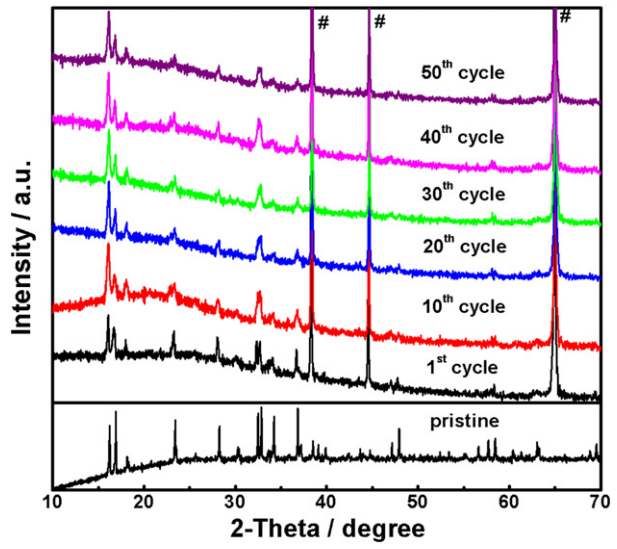

Fig. 11. XRD patterns of pristine Li_2CoPO_4F (SG) sample and Li_2CoPO_4F (SG) electrodes after different cycles. The diffraction peaks corresponding to Al current collector are marked by the symbols #.

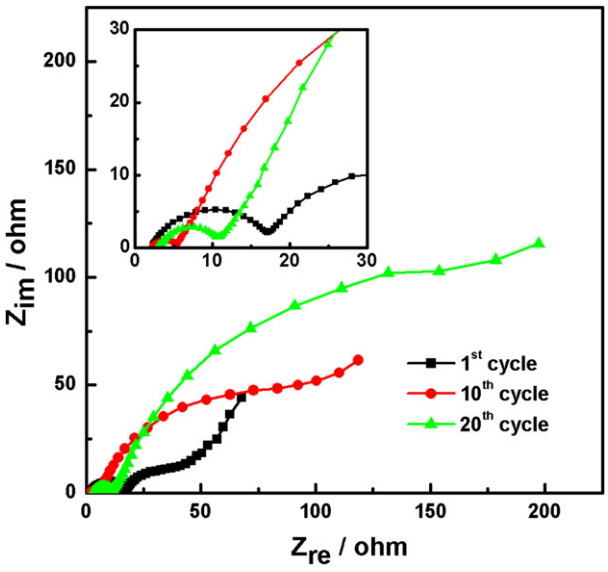

Fig. 12. Nyquist plots of Li_2CoPO_4F (SG)/Li half cell in $LiPF_6$/EC + DMC electrolyte at different cycles. The data were collected at the charged state of 4.9 V.

that of Li_2CoPO_4F (SG)/Li half cells. The poor cycling performance of Li_2CoPO_4F (SG)/$Li_4Ti_5O_{12}$ full cells may be attributed to the degradation of Li_2CoPO_4F cathode material and/or the consumption of $Li_4Ti_5O_{12}$ anode material compensating the irreversible capacity during charging. As we have noticed, coulombic efficiency of Li_2CoPO_4F (SG)/$Li_4Ti_5O_{12}$ full cells is relatively low, especially in the first several cycles. If the irreversible capacity is only compensated by consumption of $Li_4Ti_5O_{12}$ anode material, the cycling performance of Li_2CoPO_4F (SG)/$Li_4Ti_5O_{12}$ full cells would be much worse (the capacity would quickly decrease close to 0 mAh g^{-1}) than the obtained data. Therefore, there is at least another way to compensate the irreversible capacity during charging. It is speculated that the decomposition products of electrolyte are reduced on the $Li_4Ti_5O_{12}$ anode during charging process. This phenomenon is also observed in $LiCoMnO_4$/$Li_4Ti_5O_{12}$ full cell (capacity limited by $Li_4Ti_5O_{12}$) that the first charge capacity is up to 256 mAh g^{-1}

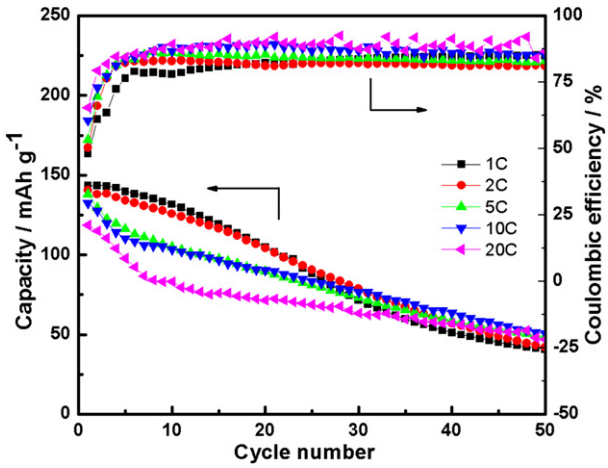

Fig. 13. Cycling performance and coulombic efficiency plots of Li_2CoPO_4F (SG)/$Li_4Ti_5O_{12}$ full cells in $LiPF_6$/EC + DMC electrolyte at various rates.

[25]. Further research is needed to disclose the detailed reaction mechanism.

4. Conclusions

Li_2CoPO_4F/C nanocomposite cathode material is successfully synthesized by a sol–gel method. It can be observed from SEM and TEM images that the primary particle of the composites is only tens of nanometers and coated by an amorphous carbon layer, which results in remarkable improvement in electrochemical performance compared with the sample prepared by solid state method. Li_2CoPO_4F/C cathode material prepared by sol–gel process exhibits discharge capacities of 138 mAh g^{-1}, 135 mAh g^{-1}, 133 mAh g^{-1}, 127 mAh g^{-1} and 119 mAh g^{-1} at current rates of 1 C, 2 C, 5 C, 10 C and 20 C, respectively. The high working voltage, high theoretical capacity and high rate performance make Li_2CoPO_4F a promising cathode material with high energy density and power density for lithium ion battery. Our results also show that $Li_2CoPO_4F/Li_4Ti_5O_{12}$ full cells deliver similar discharge capacity to Li_2CoPO_4F/Li half cells and excellent power density. Consequently, $Li_2CoPO_4F/Li_4Ti_5O_{12}$ full cell can become another candidate for high power battery. However, Li_2CoPO_4F cathode material suffers from poor cycling performance, which may be due to the increased charge-transfer resistance resulting from the deterioration of electrode/electrolyte interface.

Acknowledgments

We are grateful for the sponsors of the research reported in this paper: National Basic Research Program of China (973 program, Grant No. 2011CB935903) and the National Natural Science Foundation of China (Grant Nos. 21021002 and 20873115).

References

[1] J.M. Tarascon, Philos. Trans. R. Soc. 368 (2010) 3227–3241.
[2] A.K. Padhi, K.S. Nanjundaswamy, J.B. Goodenough, J. Electrochem. Soc. 144 (1997) 1188–1194.
[3] J.B. Goodenough, Y. Kim, Chem. Mater. 22 (2009) 587–603.
[4] P.G. Bruce, B. Scrosati, J.-M. Tarascon, Angew. Chem. Int. Ed. 47 (2008) 2930–2946.
[5] P. Reale, S. Panero, B. Scrosati, J. Garche, M. Wohlfahrt-Mehrens, M. Wachtler, J. Electrochem. Soc. 151 (2004) A2138–A2142.
[6] N. Recham, J.N. Chotard, J.C. Jumas, L. Laffont, M. Armand, J.M. Tarascon, Chem. Mater. 22 (2010) 1142–1148.
[7] B.L. Ellis, W.R.M. Makahnouk, W.N. Rowan-Weetaluktuk, D.H. Ryan, L.F. Nazar, Chem. Mater. 22 (2010) 1059–1070.
[8] N. Recham, J.N. Chotard, L. Dupont, K. Djellab, M. Armand, J.M. Tarascon, J. Electrochem. Soc. 156 (2009) A993–A999.
[9] B.L. Ellis, W.R.M. Makahnouk, Y. Makimura, K. Toghill, L.F. Nazar, Nat. Mater. 6 (2007) 749–753.
[10] S. Okada, M. Ueno, Y. Uebou, J.-i. Yamaki, J. Power Sources 146 (2005) 565–569.
[11] O.V. Yakubovich, O.V. Karimova, O.K. Melnikov, Acta Crystallogr. C 53 (1997) 395–397.
[12] X. Wu, J. Zheng, Z. Gong, Y. Yang, J. Mater. Chem. 21 (2011) 18630–18637.
[13] N.R. Khasanova, A.N. Gavrilov, E.V. Antipov, K.G. Bramnik, H. Hibst, J. Power Sources 196 (2011) 355–360.
[14] D.Y. Wang, J. Xiao, W. Xu, Z.M. Nie, C.M. Wang, G. Graff, J.G. Zhang, J. Power Sources 196 (2011) 2241–2245.
[15] J. Hadermann, A.M. Abakumov, S. Turner, Z. Hafideddine, N.R. Khasanova, E.V. Antipov, G. Van Tendeloo, Chem. Mater. 23 (2011) 3540–3545.
[16] N.V. Kosova, E.T. Devyatkina, A.B. Slobodyuk, Solid State Ion. (2011). http://dx.doi.org/10.1016/j.ssi.2011.1011.1007.
[17] E. Dumont-Botto, C. Bourbon, S. Patoux, P. Rozier, M. Dolle, J. Power Sources 196 (2011) 2274–2278.
[18] A. Nyten, A. Abouimrane, M. Armand, T. Gustafsson, J.O. Thomas, Electrochem. Commun. 7 (2005) 156–160.
[19] Z. Gong, Y. Yang, Energy Environ. Sci. 4 (2011) 3223–3242.
[20] C. Lyness, B. Delobel, A.R. Armstrong, P.G. Bruce, Chem. Commun. (2007) 4890–4892.
[21] A. von Cresce, K. Xu, J. Electrochem. Soc. 158 (2011) A337–A342.
[22] K. Kiyoshi, J. Power Sources 81–82 (1999) 123–129.
[23] K. Xu, C.A. Angell, J. Electrochem. Soc. 149 (2002) A920–A926.
[24] E. Markevich, R. Sharabi, H. Gottlieb, V. Borgel, K. Fridman, G. Salitra, D. Aurbach, G. Semrau, M.A. Schmidt, N. Schall, C. Bruenig, Electrochem. Commun. 15 (2012) 22–25.
[25] X. Huang, M. Lin, Q. Tong, X. Li, Y. Ruan, Y. Yang, J. Power Sources 202 (2012) 352–356.